AIChE

High-Order Simulation of Polymorphic Crystallization Using Weighted Essentially Nonoscillatory Methods

Martin Wijaya Hermanto
Dept. of Chemical and Biomolecular Engineering, National University of Singapore, Singapore 117576

Richard D. Braatz
Dept. of Chemical and Biomolecular Engineering, University of Illinois at Urbana-Champaign, IL 61801

Min-Sen Chiu
Dept. of Chemical and Biomolecular Engineering, National University of Singapore, Singapore 117576

DOI 10.1002/aic.11644
Published online November 21, 2008 in Wiley InterScience (www.interscience.wiley.com).

Most pharmaceutical manufacturing processes include a series of crystallization processes to increase purity with the last crystallization used to produce crystals of desired size, shape, and crystal form. The fact that different crystal forms (known as polymorphs) can have vastly different characteristics has motivated efforts to understand, simulate, and control polymorphic crystallization processes. This article proposes the use of weighted essentially nonoscillatory (WENO) methods for the numerical simulation of population balance models (PBMs) for crystallization processes, which provide much higher order accuracy than previously considered methods for simulating PBMs, and also excellent accuracy for sharp or discontinuous distributions. Three different WENO methods are shown to provide substantial reductions in numerical diffusion or dispersion compared with the other finite difference and finite volume methods described in the literature for solving PBMs, in an application to the polymorphic crystallization of L*-glutamic acid.* © 2008 American Institute of Chemical Engineers *AIChE J,* 55: 122–131, 2009

Keywords: pharmaceutical crystallization, polymorphism, hyperbolic partial differential equation, weighted essentially nonoscillatory, high resolution, finite difference

Introduction

Most manufacturing processes include a series of crystallization processes in which product quality is associated with the crystal final form (such as crystal size and shape distribution). Recently, there is a rapid growth of interest in polymorphism (when a substance has multiple crystal forms) motivated by patent, operability, profitability, regulatory, and scientific considerations.[1–3] The different polymorphs can have orders-of-magnitude differences in properties such as solubility, chemical reactivity, and dissolution rate, which can have an adverse effect on downstream operability and performance of the crystal product.[2] As a result, controlling polymorphism to ensure consistent production of the desired polymorph is very critical in those industries, including in drug manufacturing where safety is of paramount importance.

Numerical simulations for polymorphic crystallizations enable the investigation of the effects of various operating

Correspondence concerning this article should be addressed to M.-S. Chiu at checms@nus.edu.sg.

conditions and can be used for optimal design and control.[4–6] Generally, the most widely accepted approach to modelling particulate processes is based on population balance equations.[7] Solving population balance equations is particularly challenging when the partial differential equations (PDEs) are hyperbolic with sharp gradients or discontinuities in the distribution.[8] Standard first-order methods require a very small grid size in order to reduce the numerical diffusion (i.e., smearing), whereas standard higher order methods introduce numerical dispersion (i.e., spurious oscillations), which usually results in a crystal size distribution with negative values. Efficient and sufficiently accurate computational methods for simulating the population balance equations are required to ensure the behavior of the numerical solution is determined by the assumed physical principles and not by the chosen numerical method.

There have been many papers on the numerical solution of population balance models. The method of moments approximates the distribution by its moments,[9] which under certain conditions, converts the hyperbolic PDEs into a small number of ordinary differential equations (ODEs) that describe characteristics of the distribution. The method of moments does not apply to PBEs which do not satisfy moment closure conditions. The method of weighted residuals approximates the size distribution by a linear combination of basis functions,[10] which results in a system of ODEs. For most practical crystallizations, a large number of basis functions is needed to approximate the distribution, which results in high computational cost. The Monte Carlo method tracks individual particles, each of which exhibits stochastical behavior according to a probabilistic model.[11–13] This approach is too computationally expensive for most industrial crystallizations. Another problem-specific numerical method for solving population balance equations is the method of characteristics.[14,15] This method solves each population balance equation by finding curves in the characteristic size-time plane that reduce the equation to an ODE. Although the method is highly efficient when the kinetics are simple, the approach does not generalize to more complex kinetics. Most publications on numerical methods for solving PBEs involve various types of discretizations and go by a variety of names including "method of classes" and "discretized population balance equations."[16–20] In recent years there have been several efforts to reduce the numerical diffusion and numerical dispersion for distributions which contain sharp gradients or discontinuities, which is common in batch crystallizations. High-resolution (HR) finite volume methods (FVMs) popular in astrophysics and gas dynamics[21–25] were extended to the application of multidimensional population balance equations.[26–30] A typical implementation applies a first-order method near discontinuities or sharp gradients and a second-order method everywhere else, which results in less numerical dispersion than the second-order method and less numerical diffusion than the first-order method.[26]

This article considers a class of numerical algorithms known as weighted essentially nonoscillatory (WENO) methods which were developed for especially accurate simulation of shock waves and provide much higher order accuracy than the previously considered methods for solving PBMs. Three WENO methods are considered: Liu et al's version of WENO (LOCWENO),[31] Jiang and Shu's version of WENO with Henrick mapping (JSHWENO),[32,33] and the weighted power ENO method (Wpower-ENO).[34] These WENO methods are compared with the HR finite volume method and a second-order finite difference (FD2) method, for polymorphic crystallization of L-glutamic acid under conditions in which the distribution contains sharp gradients.

This article is organized as follows. First, the PBM for the polymorphic crystallization of L-glutamic acid is summarized. Then the five numerical methods are discussed and compared. Finally, conclusions are provided.

Process Model

This section presents a kinetic model for the polymorphic crystallization of metastable α-form and stable β-form crystals of L-glutamic acid (Hermanto et al.[35]). The population balance equations are

$$\frac{\partial f_{\text{seed},i}}{\partial t} + \frac{\partial (G_i f_{\text{seed}}, i)}{\partial L} = 0, \tag{1}$$

$$\frac{\partial f_{\text{nucl},i}}{\partial t} + \frac{\partial \left(G_i f_{\text{nucl},i}\right)}{\partial L} = B_i \delta(L - L_0), \tag{2}$$

where $f_{\text{seed},i}$ and $f_{\text{nucl},i}$ are the crystal size distributions of the i-form crystals (i.e., α- or β-form crystals) obtained from seed crystals and nucleated crystals (#m^{-4}), B_i and G_i are the nucleation (#m^3 s^{-1}) and growth rate (m s^{-1}) of the i-form crystals, L and L_0 are the characteristic size of crystals (m) and nuclei (m), and $\delta(\cdot)$ is a Dirac delta function. These equations are augmented by the solute mass balance:

$$\frac{dC}{dt} = -3\frac{10^3}{\rho_{\text{solv}}}\left(\rho_\alpha k_{v\alpha} G_\alpha \mu_{\alpha,2} + \rho_\beta k_{v\beta} G_\beta \mu_{\beta,2}\right), \tag{3}$$

where the nth moment of the i-form crystals (#m^{n-3}) is

$$\mu_{i,n} = \int_0^\infty L^n \left(f_{\text{nucl},i} + f_{\text{seed},i}\right) dL, \tag{4}$$

C is the solute concentration (g kg^{-1}), ρ_{solv} is the density of the solvent (kg m^{-3}), ρ_i is the density of the i-form crystals (kg m^{-3}), k_{vi} is the volumetric shape factor of the i-form crystals (dimensionless) as defined by $v_i = k_{vi} L^3$, where v_i is the volume of the i-form crystal (m^3), and 10^3 is a constant (g kg^{-1}) to ensure unit consistency. The kinetic expressions are

$$B_\alpha = k_{b\alpha}(S_\alpha - 1)\mu_{\alpha,3} \quad (\alpha\text{-form crystal nucleation rate}), \tag{5}$$

$$G_\alpha = \begin{cases} k_{g\alpha}(S_\alpha - 1)^{g_\alpha} & \text{if } S_\alpha \geq 1 \\ & (\alpha\text{-form crystal growth/ dissolution rate}), \\ k_{d\alpha}(S_\alpha - 1) & \text{otherwise} \end{cases} \tag{6}$$

$$B_\beta = k_{b\beta,1}\left(S_\beta - 1\right)\mu_{\alpha,3} + k_{b\beta,2}\left(S_\beta - 1\right)\mu_{\beta,3} \quad (\beta\text{-form crystal nucleation rate}), \tag{7}$$

$$G_\beta = k_{g\beta,1}\left(S_\beta - 1\right)^{g_\beta} \exp\left(-\frac{k_{g\beta,2}}{S_\beta - 1}\right) \quad (\beta\text{-form crystal growth rate}), \tag{8}$$

Table 1. Model Parameters for L-glutamic Acid Polymorphic Crystallization

Parameters	Values	Parameters	Values
$\ln(k_{b\alpha})$	17.233	ρ_{solv}	990
$\ln(k_{g\alpha,0})$	1.878	$\rho_\alpha = \rho_\beta$	1540
g_α	1.859	$k_{v\alpha}$	0.480
$\ln(E_{g\alpha})$	10.671	$k_{v\beta}$	0.031
$\ln(k_{d\alpha})$	−10.260	$a_{\alpha,1}$	8.437×10^{-3}
$\ln(k_{b\beta,1})$	15.801	$a_{\alpha,2}$	3.032×10^{-2}
$\ln(k_{b\beta,2})$	20.000	$a_{\alpha,3}$	4.564
$\ln(k_{g\beta,0})$	52.002	$a_{\beta,1}$	7.644×10^{-3}
$\ln(k_{g\beta,2})$	−0.251	$a_{\beta,2}$	-1.165×10^{-1}
g_β	1.047	$a_{\beta,3}$	6.622
$\ln(E_{g\beta})$	12.078		

where $S_i = C/C_{sat,i}$ and $C_{sat,i} = a_{i,1}T^2 + a_{i,2}T + a_{i,3}$ are the supersaturation and the saturation concentration (g kg^{-1}) of the i-form crystals, respectively, and T is the solution temperature (°C). The kinetic parameters $k_{b\alpha}$, $k_{g\alpha}$, and $k_{d\alpha}$ correspond to the nucleation (#m^{-3} s^{-1}), growth (m s^{-1}), and dissolution (m s^{-1}) rates of α-form crystals, respectively, whereas $k_{b\beta,j}$ and $k_{g\beta,j}$ correspond to the jth nucleation (#m^{-3} s^{-1}) and growth (m s^{-1}) for $j = 1$ and dimensionless for $j = 2$ rates of β-form crystals, respectively, and g_i is the growth exponential constant of the i-form crystals which may have a value between 1 (for diffusion-limited growth) and 2 (for surface integration-limited growth).[36] The Arrhenius equation was used to account for the variability of crystal growth rate with temperature:

$$k_{g\alpha} = k_{g\alpha,0}\exp\left(-\frac{E_{g\alpha}}{8.314(T+273)}\right), \tag{9}$$

$$k_{g\beta,1} = k_{g\beta,0}\exp\left(-\frac{E_{g\beta}}{8.314(T+273)}\right), \tag{10}$$

where $k_{gi,0}$ and E_{gi} are the pre-exponential factor (m s^{-1}) and activation energy (J mol^{-1}) for the growth rate of i-form crystals, respectively. The values for densities, volumetric shape factors, and parameters for the saturation concentration are in Table 1.

Secondary nucleation is assumed for both α- and β-form crystals, since it is the dominant nucleation process in seeded crystallization. The growth rate expression for the α-form crystals includes both growth (supersaturation) and dissolution (undersaturation). Dissolution occurs during the polymorphic transformation of α- to β-form crystals, where α-form crystals dissolve and β-form crystals nucleate and grow.

Numerical Methods

The numerical methods described here differ in terms of their discretization along the crystal size dimension (L), each of which produces a system of ODEs describing the time evolution of the crystal size distribution at the chosen discretized points L_k.[37] To provide a fair basis for comparison, the implementation of all of the methods integrated the ODEs using a fourth-order orthogonal Runge-Kutta Chebyshev method,[38] which is a class of explicit Runge-Kutta methods with extended stability domains along the negative real axis. The stability properties of this method make it suitable for stiff problems.

It is advantageous for a numerical method to be *conservative*, that is, to ensure that a quantity remains conserved by calculating a single flux which describes the flow of that quantity between neighbouring cells.[22,23] Although flux conservative schemes are normally formulated using finite volumes, a finite difference scheme is utilized here based on the approach described in Shu.[39]

$$\frac{\partial f_{nucl,i}}{\partial t} + \frac{\partial\left(G_i f_{nucl,i}\right)}{\partial L} = 0, \tag{11}$$

$$f_{nucl,i}(L_0, t) = \frac{B_i}{G_i}. \tag{12}$$

To simplify notation, (1) and (11) are written in the same form

$$\begin{aligned} \frac{\partial u}{\partial t} + \frac{\partial p}{\partial L} &= 0, \\ \frac{\partial u}{\partial t} &= -\frac{\partial p}{\partial L}, \end{aligned} \tag{13}$$

where u is $f_{seed,i}$ or $f_{nucl,i}$ and p is $G_i f_{seed,i}$ or $G_i f_{nucl,i}$. Equation 13 is discretized in the L domain with uniform intervals of size ΔL, $L_k = k\ \Delta L$ indicates the crystal size at node k, and $I_k = [L_{k-1/2}, L_{k+1/2}]$ is the k^{th} cell. The conservative approximation to the spatial derivative is used:

$$\frac{du_k(t)}{dt} = -\frac{1}{\Delta L}\left(\hat{p}_{k+1/2} - \hat{p}_{k-1/2}\right), \tag{14}$$

where u_k is the value of u at L_k and the numerical flux $\hat{p}_{k+1/2}$ approximates $h_{k+1/2} = h(L_{k+1/2})$ with $h(L)$ implicitly defined by[39]

$$p(u(L)) = \frac{1}{\Delta L}\int_{L-\Delta L/2}^{L+\Delta L/2} h(\xi)\, d\xi. \tag{15}$$

For stability, it is important that upwinding is used in constructing the numerical flux $\hat{p}_{k+1/2}$. One way is to compute the Roe speed to determine the direction of the wind:

$$\bar{a}_{k+1/2} = \frac{p_{k+1} - p_k}{u_{k+1} - u_k}, \tag{16}$$

where p_k is the value of p at L_k.

In the context of process model, the Roe speed is

$$\bar{a}_{k+1/2} \approx G_i, \tag{17}$$

and

- if $G_i \geq 0$ then the wind blows from the left to the right and the numerical fluxes $\hat{p}_{k+1/2}$ and $\hat{p}_{k-1/2}$ are approximated by $p^-_{k+1/2}$ and $p^-_{k-1/2}$, respectively.
- if $G_i < 0$ then the wind blows from the right to the left and the numerical fluxes $\hat{p}_{k+1/2}$ and $\hat{p}_{k-1/2}$ are approximated by $p^+_{k+1/2}$ and $p^+_{k-1/2}$, respectively.

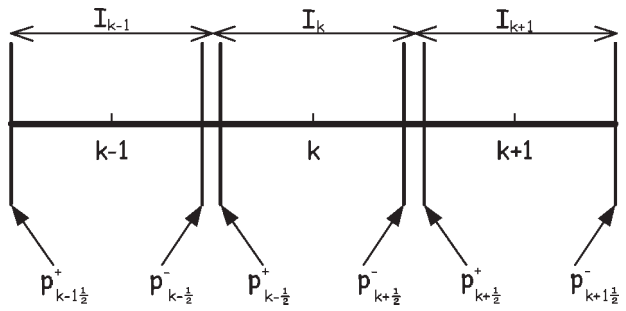

Figure 1. Computational cells.

The difference between the values with superscript $\pm$ at the same location $L_{k+1/2}$ is due to the possibility of different stencils for cell I_k and for cell I_{k+1}, that is, $p^-_{k+1/2}$ is due to the stencil for cell I_k and $p^+_{k+1/2}$ is due to the stencil for cell I_{k+1} (see Figure 1). In the next sections, five reconstruction procedures are described to obtain $p^-_{k-1/2}$ and $p^+_{k+1/2}$ only, as $p^+_{k+1/2}$ can be readily derived from $p_{k\prime-1/2}+$ for cell $I_{k'} = I_{k+1}$ and $p^-_{k-1/2}$ can be derived from $p^-_{k'+1/2}$ for cell $I_{k'} = I_{k-1}$.

WENO variants

All WENO methods discussed here are the derivatives of the original essentially nonoscillatory (ENO) method developed by Harten et al.[41] in 1987. This article was the first to obtain a self similar (i.e., no mesh size-dependent parameter), uniformly high order accurate, yet essentially nonoscillatory interpolation [i.e., the magnitude of the oscillations decays as $O(\Delta x^r)$ where r is the order of accuracy] for piecewise smooth functions. ENO methods are especially suitable for problems containing both shocks and complicated smooth flow structures, such as those occurring in shock interactions with a turbulent flow and shock interaction with vortices. To improve the ENO method and further expand its applications, ENO methods based on point values and total diminishing variation (TVD) Runge-Kutta time discretizations were developed, which can reduce computational costs significantly for multiple space dimensions.[39,40] Then biasing during selection of the stencil was proposed for enhancing stability and accuracy.[42,43] Later, WENO methods were developed, using a convex combination of all candidate stencils instead of just one as in the original ENO.[31–34]

WENO methods improve the accuracy of the original ENO method to the optimal order in smooth regions while maintaining the essentially nonoscillatory property near discontinuities. Liu et al.[31] converted the rth order ENO method into an $(r+1)$th order WENO method with a cell average approach. Based on the pointwise finite difference ENO method[39,40] and a new smoothness indicator, the WENO method by Jiang and Shu[32] can achieve the optimal $(2r-1)$th order accuracy. Jiang and Shu's WENO version was later modified by adding a mapping function for the original nonlinear weight which improves accuracy near smooth extrema.[33] Serna and Marquina[34] improved the behavior of Jiang and Shu's WENO method by introducing the powereno$_3$ or powermod$_3$ limiter, resulting in an $(2r-1)$th order weighted power ENO method. The powereno$_3$ or powermod$_3$ limiter substantially reduces smearing near discontinuities and results in better resolution of corners and local extrema.

All WENO methods adopt the following idea. Denote the r candidate stencils by

$$S_m = (L_{k+m-r+1}, L_{k+m-r+2}, \ldots, L_{k+m}), \quad m = 0, 1, \ldots, r-1, \tag{18}$$

whose corresponding rth order ENO approximation of the flux $h_{k+1/2}$ is

$$p^-_{k+1/2} = q^r_m(p_{k+m-r+1}, \ldots, p_{k+m})\big|_{L=L_{k+1/2}}. \tag{19}$$

Using the smoothest stencil among the r candidates for the approximation of $h_{k+1/2}$ is desirable near discontinuities to avoid introducing aphysical oscillations. All of the stencils are smooth in regions where the solution is smooth, in which case it is better to combine the results of multiple stencils together to produce a higher order (higher than rth order, the order of the original ENO method) approximation to the flux $h_{k+1/2}$.[32] WENO methods assign a weight ω_m to each candidate stencil S_m to obtain the combined approximation of $h_{k+1/2}$ as

$$p^-_{k+1/2} = \sum_{m=0}^{r-1} \omega_m q^r_m(p_{k+m-r+1}, \ldots, p_{k+m})\big|_{L=L_{k+1/2}}. \tag{20}$$

To achieve the essentially nonoscillatory property, the weights adapt to the relative smoothness of p on each candidate stencil such that any discontinuous stencil is effectively assigned a zero weight. In smooth regions the weights are adjusted such that the resulting approximation gives an order of accuracy higher than r. The differences between WENO methods lie on the method for selecting the weights ω_m and the flux approximations $q^r_m(p_{k+m-r+1},\ldots,p_{k+m})$. The subsequent WENO methods have $r = 3$ with the flux approximations $q^r_m(p_{k+m-r+1},\ldots,p_{k+m})$ constructed based on quadratic polynomials.

Liu et al.'s WENO (LOCWENO) method

The flux approximations and weights for the fourth-order accurate LOCWENO method are[31]

$$\begin{aligned} q^3_m(p_{k+m-2}, p_{k+m-1}, p_{k+m}) &= \frac{p_{k+m} - 2p_{k+m-1} + p_{k+m-2}}{2\Delta L}(L - L_{k+m-1})^2 \\ &\quad + \frac{p_{k+m} - p_{k+m-2}}{2\Delta L}(L - L_{k+m-1}) \\ &\quad + p_{k+m-1} - \frac{p_{k+m} - 2p_{k+m-1} + p_{k+m-2}}{24} \end{aligned} \tag{21}$$

and

$$\omega_m = \frac{\lambda_m}{\sum_{j=0}^{2} \lambda_j}, \tag{22}$$

Table 2. Values of h and d_m for LOCWENO, JSHWENO, and WPower-ENO Methods

	LOCWENO	JSHWENO	WPower-ENO
h	3	2	2
d_0	1/12	1/10	1/5
d_1	1/2	3/5	1/5
d_2	1/4	3/10	2/5

where

$$\lambda_m = \begin{cases} \dfrac{d_m}{(IS_m+\varepsilon)^h} & \text{for } p^-_{k+1/2} \\ \dfrac{d_{2-m}}{(IS_m+\varepsilon)^h} & \text{for } p^+_{k-1/2}. \end{cases} \tag{23}$$

The values of h and d_m in Eq. 23 are in Table 2 and ε is a small number to avoid division by zero (i.e., $\varepsilon = 10^{-4}$ was used in this article). The IS_m are smoothness indicators given by

$$\mathrm{IS}_m = \frac{(p_{k+m-1}-p_{k+m-2})^2 + (p_{k+m}-p_{k+m-1})^2}{2} + (p_{k+m}-2p_{k+m-1}+p_{k+m-2})^2. \tag{24}$$

Jiang and Shu's WENO method with Henrick mapping (JSHWENO)

The Jiang and Shu's WENO method used here is based on the quadratic polynomial instead of the original linear approximation. With

$$d_{k+1/2} = p_{k+1} - p_k, \tag{25}$$

$$d_k = \frac{d_{k+1/2}+d_{k-1/2}}{2}, \tag{26}$$

$$D_k = d_{k+1/2} - d_{k-1/2}, \tag{27}$$

the flux approximations are

$$q^3_0(p_{k-2},p_{k-1},p_k) = p_k - \frac{D_{k-1}}{24} + \frac{(L-L_k)}{\Delta L}\left[d_{k-1/2} + \frac{D_{k-1}}{2} + \frac{D_{k-1}}{2}\left(\frac{L-L_k}{\Delta L}\right)\right], \tag{28}$$

$$q^3_1(p_{k-1},p_k,p_{k+1}) = p_k - \frac{D_k}{24} + \frac{(L-L_k)}{\Delta L}\left[d_k + \frac{D_k}{2}\left(\frac{L-L_k}{\Delta L}\right)\right], \tag{29}$$

$$q^3_2(p_k,p_{k+1},p_{k+2}) = p_k - \frac{D_{k+1}}{24} + \frac{(L-L_k)}{\Delta L}\left[d_{k+1/2} - \frac{D_{k+1}}{2} + \frac{D_{k+1}}{2}\left(\frac{L-L_k}{\Delta L}\right)\right], \tag{30}$$

and the weights are[32]

$$\omega^{JS}_m = \frac{\lambda_m}{\sum_{j=0}^2 \lambda_j}, \tag{31}$$

where λ_m is defined in Eq. 23 and the values of h and d_m are in Table 2. The smoothness indicators IS_m are

$$\mathrm{IS}_0 = \frac{13}{12}(p_{k-2}-2p_{k-1}+p_k)^2 + \frac{1}{4}(p_{k-2}-4p_{k-1}+3p_k)^2, \tag{32}$$

$$\mathrm{IS}_1 = \frac{13}{12}(p_{k-1}-2p_k+p_{k+1})^2 + \frac{1}{4}(p_{k-1}-p_{k+1})^2, \tag{33}$$

$$\mathrm{IS}_2 = \frac{13}{12}(p_k-2p_{k+1}+p_{k+2})^2 + \frac{1}{4}(3p_k-4p_{k+1}+p_{k+2})^2. \tag{34}$$

The Henrick mapping[33]

$$g_m(\omega) = \frac{\omega(d_m+d_m^2-3d_m\omega+\omega^2)}{d_m^2+(1-2d_m)\omega}. \tag{35}$$

is used to revise these weights to improve the accuracy near smooth extrema:

$$\omega^{HJS}_m = \frac{\lambda^*_m}{\sum_{j=0}^2 \lambda^*_j} \tag{36}$$

with

$$\lambda^*_m = g_m(\omega^{JS}_m), \tag{37}$$

to produce a fifth-order accurate method.

Weighted power ENO (Wpower-ENO) method

Using the definitions in Eqs. 25–27, the flux approximations for the Wpower-ENO method are

$$q^3_0(p_{k-2},p_{k-1},p_k) = p_k - \frac{Pow_{k-1/2}}{24} + \frac{(L-L_k)}{\Delta L}\left[d_{k-1/2} + \frac{Pow_{k-1/2}}{2} + \frac{Pow_{k-1/2}}{2}\left(\frac{L-L_k}{\Delta L}\right)\right], \tag{38}$$

$$q^3_1(p_{k-1},p_k,p_{k+1}) = p_k - \frac{D_k}{24} + \frac{(L-L_k)}{\Delta L}\left[d_k + \frac{D_k}{2}\left(\frac{L-L_k}{\Delta L}\right)\right], \tag{39}$$

$$q^3_2(p_k,p_{k+1},p_{k+2}) = p_k - \frac{Pow_{k+1/2}}{24} + \frac{(L-L_k)}{\Delta L}\left[d_{k+1/2} - \frac{Pow_{k+1/2}}{2} + \frac{Pow_{k+1/2}}{2}\left(\frac{L-L_k}{\Delta L}\right)\right], \tag{40}$$

where

$$Pow_{k+1/2} = \mathrm{powereno}_3(D_k, D_{k+1}), \tag{41}$$

is the powereno limiter acting on $L = L_{k+1/2}$ where

$$\mathrm{powereno}_3(x,y) = \mathrm{minsign}(x,y)\cdot \mathrm{power}_3(|x|,|y|)\ , \tag{42}$$

$$\mathrm{minsign}(x,y) = \begin{cases} \mathrm{sign}(x) & \text{if } |x| \le |y|\ , \\ \mathrm{sign}(y) & \text{otherwise}\ , \end{cases} \tag{43}$$

Table 3. Initial Seed Distribution Parameters for α- and β-forms

i	κ_i	$\sigma_{\text{seed},i}[\text{m}] \times 10^6$	$\hat{L}_{\text{seed},i}[\text{m}] \times 10^6$
α	2×10^{10}	2.000	30.000
β	2×10^{10}	4.000	50.000

$$\text{power}_3(x,y) = \min(x,y)\frac{x^2+y^2+2[\max(x,y)]^2}{(x+y)^2}\ . \quad (44)$$

The weights ω_m and parameters λ_m are the same as for the LOCWENO method, except that the smoothness indicators

$$\text{IS}_0 = \frac{13}{12}\left(Pow_{k-1/2}\right)^2 + \frac{1}{4}\left(2p_k - 2p_{k-1} + Pow_{k-1/2}\right)^2, \quad (45)$$

$$\text{IS}_1 = \frac{13}{12}(p_{k-1} - 2p_k + p_{k+1})^2 + \frac{1}{4}(p_{k-1} - p_{k+1})^2, \quad (46)$$

$$\text{IS}_2 = \frac{13}{12}\left(Pow_{k+1/2}\right)^2 + \frac{1}{4}\left(2p_{k+1} - 2p_k - Pow_{k+1/2}\right)^2, \quad (47)$$

are used. This method is fifth-order accurate.

HR method

The popular HR method uses second-order discretization with a flux limiter to ensure nonoscillatory behavior. For $G_i \geq 0$, a backward second-order discretization is used:

$$p^-_{k+1/2} - p^-_{k-1/2} = \frac{1}{2}(3p_k - 4p_{k-1} + p_{k-2}) = \frac{1}{2}(3p_k - p_{k-1}) - \frac{1}{2}(3p_{k-1} - p_{k-2}) \quad (48)$$

or

$$p^-_{k+1/2} = \frac{1}{2}(3p_k - p_{k-1}) = p_k + \frac{1}{2}(p_k - p_{k-1})\ , \quad (49)$$

where the first term is first-order and the second term is commonly referred to as an "anti-diffusion term" because it reduces numerical diffusion. Applying a flux limiter on the antidiffusion term yields

$$p^-_{k+1/2} = p_k + \frac{1}{2}\phi(w_k)(p_k - p_{k-1})\ , \quad (50)$$

where w_k is the upwinding ratio defined by

$$w_k = \frac{p_{k+1} - p_k}{p_k - p_{k-1}} \quad (51)$$

and $\phi(\cdot)$ is the flux limiter. In this article, the popular Van Leer flux limiter[44] was used:

$$\phi(w) = \frac{w + |w|}{1 + w}\ . \quad (52)$$

For $G_i < 0$, a forward second-order discretization is used:

$$p^+_{k+1/2} - p^+_{k-1/2} = \frac{1}{2}(-3p_k + 4p_{k+1} - p_{k+2}) = \frac{1}{2}(-p_{k+2} + 3p_{k+1}) - \frac{1}{2}(-p_{k+1} + 3p_k) \quad (53)$$

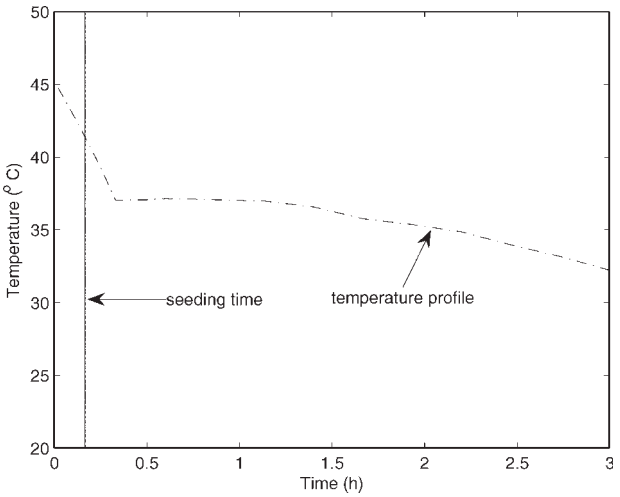

Figure 2. Temperature profile used in simulations.

or

$$p^+_{k-1/2} = \frac{1}{2}(3p_k - p_{k+1}) = p_k - \frac{1}{2}(p_{k+1} - p_k) \quad (54)$$

Similar inclusion of a flux limiter to the antidiffusion term gives

$$p^+_{k-1/2} = p_k - \frac{1}{2}\phi\left(\frac{1}{w_k}\right)(p_{k+1} - p_k). \quad (55)$$

This HR method is second-order accurate in smooth regions, and first-order accurate near discontinuities.

The second-order finite difference (FD2) method

A second-order finite difference method with correct upwinding uses the fluxes $p^-_{k+1/2}$ and $p^+_{k+1/2}$ given by Eq. 49 and 54, respectively.

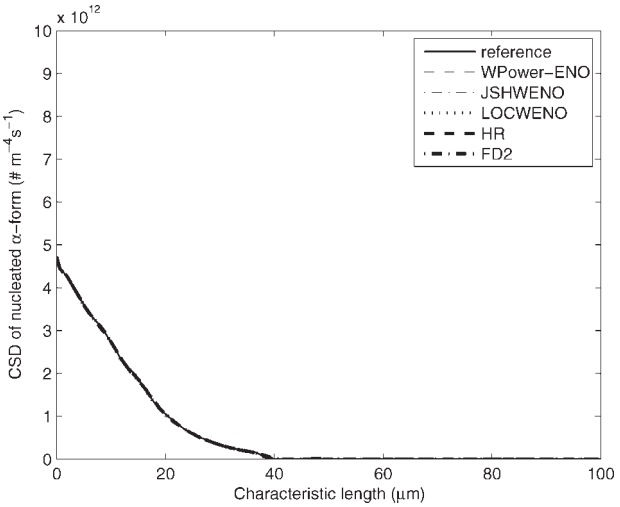

Figure 3. CSD of nucleated α form at the end of the batch for the various numerical methods (ΔL = 0.6 μm).

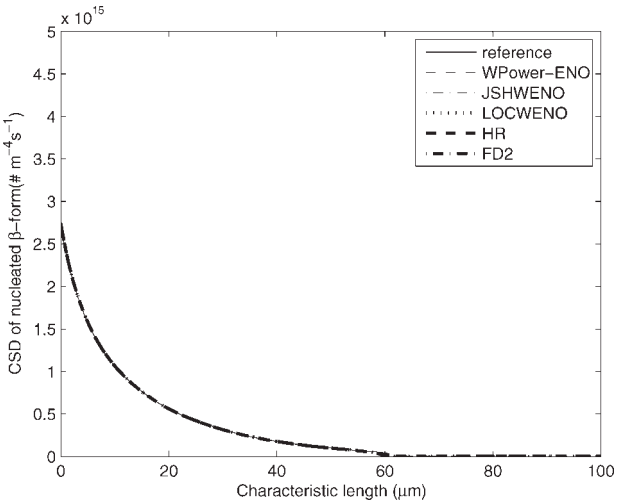

Figure 4. CSD of nucleated β form at the end of the batch for the various numerical methods (ΔL = 0.6 μm).

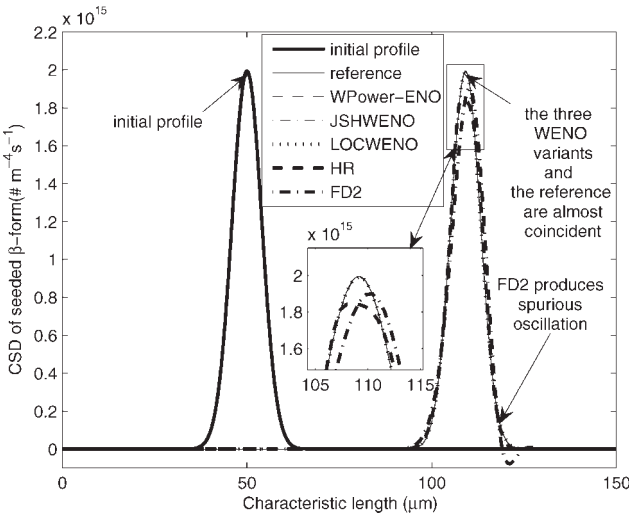

Figure 6. CSD of seeded β form at the end of the batch for the various numerical methods (ΔL = 0.6 μm).

Simulation Results

The five numerical methods were applied to the L-glutamic acid polymorphic crystallization model. The initial seed distributions $f_{\text{seed},i}(L,0)$ for α- and β-forms are described by Gaussian distributions:

$$f_{\text{seed},i}(L,0) = \frac{\kappa_i}{\sqrt{2\pi}\sigma_{\text{seed},i}} \exp\left(-\frac{(L-\hat{L}_{\text{seed},i})^2}{2\sigma^2_{\text{seed},i}}\right), \qquad (56)$$

with the parameters in Table 3 selected so that the distributions would be sharp enough to challenge numerical methods. The temperature profile is in Figure 2 where the vertical solid line indicates the seeding time (i.e., at t = 10 min). Since an analytical solution is not available, the reference solutions for all CSDs were obtained by using WPower-ENO method with very fine resolution. All the computations were performed using Compaq Fortran 6.6 on a HP workstation XW6400 [Intel Xeon 5150 (2.66 GHz) and 2 GB of RAM].

In an unseeded crystallization the CSD profiles for all methods are nearly coincident with the reference profiles (see Figures 3 and 4), indicating that a conventional numerical method such as FD2 might suffice, which is consistent with expectations since no sharp gradients occur in these distributions. In the case of seeded crystallization (the usual case in practice), the differences in the CSD profiles between the WENO variants and their conventional counterparts are significant (see Figures 5 and 6). While the three WENO variants are nearly indistinguishable with the reference profiles, the HR and FD2 methods exhibit numerical diffusion and do not resolve the peaks accurately. In addition, the FD2 method introduces a spurious oscillation (known as numerical disper-

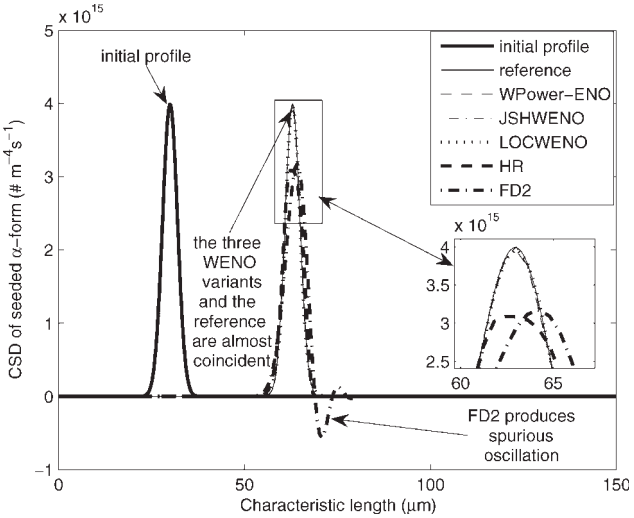

Figure 5. CSD of seeded α form at the end of the batch for the various numerical methods (ΔL = 0.6 μm).

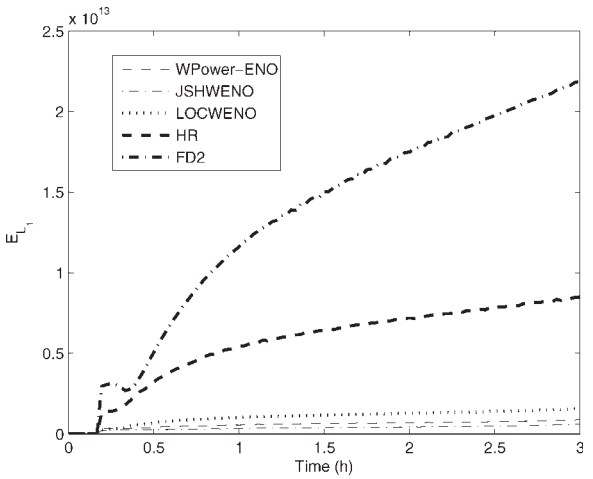

Figure 7. Evolution of the error L_1 norm with time for the various numerical methods (ΔL = 0.6 μm).

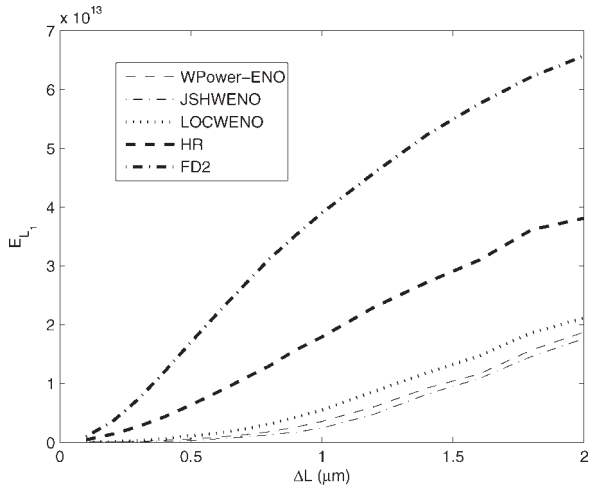

Figure 8. Error L_1 norm at the end of the batch vs. ΔL for the various numerical methods.

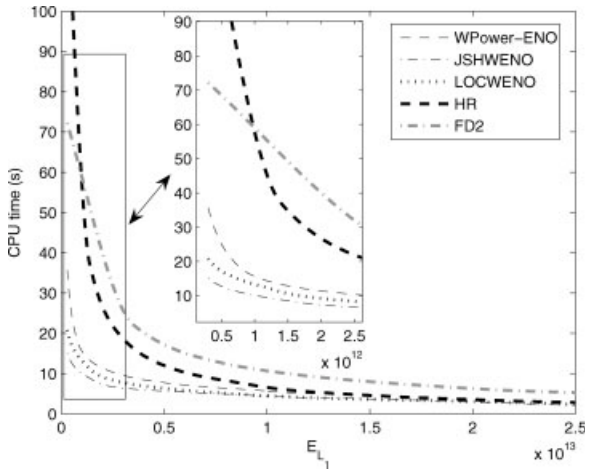

Figure 10. CPU time required for the various numerical methods for a given error L_1 norm at the end of the batch.

sion) which can occur near sharp gradients with this method. The HR method does not produce spurious oscillation because the flux limiter detects the presence of sharp gradients and limits the size derivatives. The larger numerical errors in the CSD profiles obtained by HR and FD2 methods for the seeded α-form compared with the seeded β-form are associated with its sharper gradient.

The prediction errors were quantified in terms of the L_1 norm (E_{L_1}):

$$E_{L_1} = \frac{1}{2(N_{\text{grid,seed}} + N_{\text{grid,nucl}})} \times \sum_{i=\{\alpha,\beta\}} \left\{ \sum_{k=1}^{N_{\text{grid,seed}}} \left| f_{\text{seed},i,k} - f^{\text{ref}}_{\text{seed},i,k} \right| + \sum_{k=1}^{N_{\text{grid,nucl}}} \left| f_{\text{nucl},i,k} - f^{\text{ref}}_{\text{nucl},i,k} \right| \right\}, \tag{57}$$

where $f^{\text{ref}}_{\text{seed},i,k}$ and $f^{\text{ref}}_{\text{nucl},i,k}$ are the reference solutions for the seeded and nucleated crystals size distributions and $N_{\text{grid,seed}}$ and $N_{\text{grid,nucl}}$ are the number of grids used to discretize the size coordinate of the seeded and nucleated crystal size distributions, respectively. The error L_1 norms from the three WENO variants are much smaller in magnitude and grow much slower than those from the HR and FD2 methods (see Figure 7). In terms of the L_1 norm, the JSHWENO method gave the smallest numerical errors. Figure 8 indicates that the JSHWENO method gave smaller numerical errors for the full range of ΔL from 0.1 to 2.0 μm.

The JSHWENO method generally had lower CPU times than the WPower-ENO method, but somewhat higher CPU times than the other methods for most values of ΔL (see Figure 9). To fairly compare the overall efficiency for these methods, the CPU time was compared for discretizations that produce the same error L_1 norm. From Figure 10 it is observed that, for any given error L_1 norm, the WENO variants used less or equal CPU time to the HR and FD2 meth-

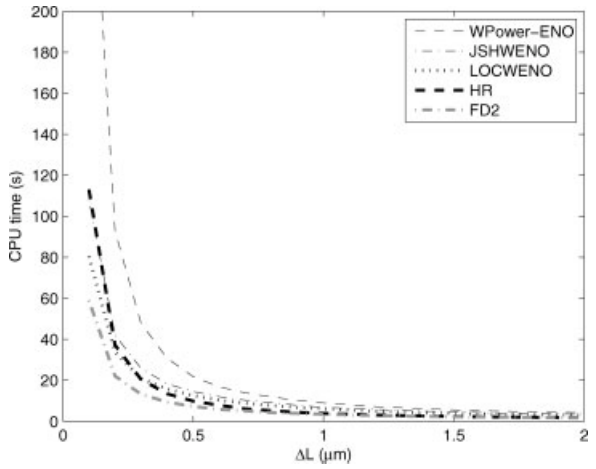

Figure 9. CPU time vs. ΔL for the various numerical methods.

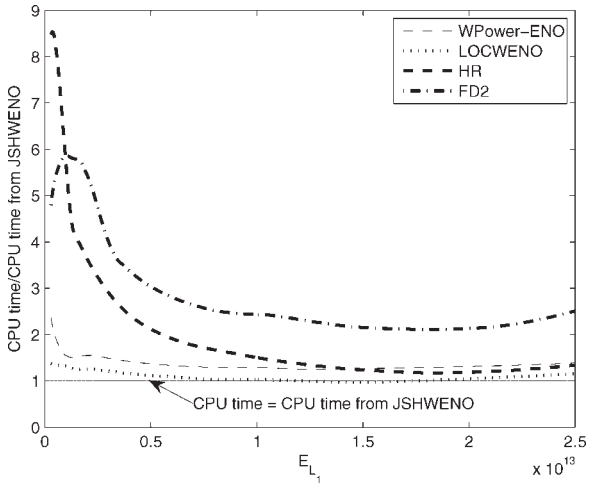

Figure 11. Relative CPU time for the various numerical methods with respect to CPU time from JSHWENO for a given error L_1 norm at the end of the batch.

Table 4. L_1 Self-convergence Order (O_{L_1}) for the Various Numerical Methods

ΔL [μm]	LOCWENO	JSHWENO	WPower-ENO	HR	FD2
0.1	1.62	1.30	1.53	1.67	1.81
0.2	2.43	1.45	1.97	1.66	1.78
0.3	2.41	2.40	2.12	1.65	1.57
0.4	2.26	2.84	2.28	1.57	1.37
0.5	2.27	2.87	2.55	1.50	1.20
0.6	2.46	2.98	2.79	1.44	1.07
0.7	2.41	3.12	2.86	1.34	0.98
0.8	2.24	3.06	2.68	1.25	0.88
0.9	2.11	3.06	2.60	1.20	0.82
1.0	1.94	2.86	2.39	1.09	0.75
Average order	*2.22*	*2.59*	*2.38*	*1.44*	*1.22*

ods, and hence the WENO variants were more efficient. The JSHWENO method was the most efficient for nearly all desired accuracy levels. Figure 11 shows the relative cost of the numerical methods with respect to the JSHWENO method. The HR method was more efficient than the FD2 method for nearly all desired accuracy levels, and was more efficient than the WPower-ENO method for some accuracy levels, but was not as efficient as the LOCWENO and JSHWENO methods. Although the WENO methods are more complicated to implement, their efficiency is much better when sufficiently high accuracy in the size distribution is desired. Among the WENO variants, the performance of JSHWENO is followed by that of the LOCWENO method by a small margin, and then followed by that of the WPower-ENO method.

Another way to assess numerical methods is to compute the L_1 self-convergence order

$$O_{L_1} = \frac{\ln\left(\frac{E_{L_1}|_{2\Delta L}}{E_{L_1}|_{\Delta L}}\right)}{\ln 2}. \tag{58}$$

This metric provides information on the internal consistency of the numerical method and its intrinsic convergence.[44] The L_1 self-convergence order for all numerical methods are in Table 4. For a linear model with a smooth solution, these values would correspond to the order of the truncation error for a given numerical method. This is not the case here because of the nonlinearity of the model and the sharp gradients in the distribution. On average, the JSHWENO method gives the best L_1 self-convergence order, followed by the WPower-ENO, LOCWENO, HR, and FD2 methods.

Conclusions

This article proposed the use of WENO methods for the numerical solution of population balance models for crystallization processes. The LOCWENO, JSHWENO, and WPower-ENO methods were compared with standard discretization methods. In simulations of the polymorphic crystallization of L-glutamic acid, the WENO methods produced much less numerical diffusion and dispersion, with the LOCWENO and JSHWENO methods having the highest overall efficiency (that is, lowest CPU time for the same level of numerical accuracy). The L_1 self-convergence order which characterizes integral consistency and convergence was the highest for the JSHWENO method, followed by the other two WENO methods. These results recommend WENO methods for the simulation of crystallization processes, especially when the distributions are sharp and very high accuracy is desired. These methods combine very high order of accuracy with good convergence properties even in the presence of sharp variation in the size distributions.

Notation

$a_{i,1}$, $a_{i,2}$, $a_{i,3}$ = parameters for the saturation concentration of the i-form crystals
$a_{k+1/2}$ = Roe speed
B_i = nucleation rate of the i-form crystals
C = solute concentration
$C_{\mathrm{sat},i}$ = saturation concentration of the i-form crystals
E_{gi} = activation energy for the growth rate of i-form crystals
E_{L_1} = prediction errors in terms of the L_1 norm
f_i, $f_{\mathrm{seed},i}$, $f_{\mathrm{nucl},i}$ = total, seed, and nucleated crystal size distribution of the i-form crystals
G_i = growth rate of the i-form crystals
I_k = the kth cell
IS_m = smoothness indicator
$k_{b\alpha}$, $k_{g\alpha}$, $k_{d\alpha}$ = nucleation, growth, and dissolution rates of α-form crystals
$k_{b\beta,j}$, $k_{g\beta,j}$ = the jth nucleation and growth rates of β-form crystals
$k_{gi,0}$ = pre-exponential factor for the growth rate of i-form crystals
k_{vi} = volumetric shape factor of the i-form crystals
L, L_0 = characteristic length of crystals and nuclei
L_k = crystals length at the kth discretized point
ΔL = discretization size of crystal length
$L_{\mathrm{seed},i}$ = mean for the seed crystal size distribution of i-form crystals
O_{L_1} = L_1 self-convergence order
$\hat{p}_{k+1/2}$, $\hat{p}_{k-1/2}$ = numerical flux approximation at node $k + 1/2$ and $k - 1/2$
q_m^r = quadratic polynomial flux approximation function
S_i = supersaturation of the i-form crystals
S_m = candidate stencil
T = crystallizer temperature

Greek letters

$\delta(\cdot)$ = dirac delta function
κ_i = scaling factor for the seed crystal size distribution of i-form crystals
$\mu_{i,n}$ = the nth moment of the i-form crystals
ω_m = scalar weight to each candidate stencil S_m for the flux approximation
ϕ = flux limiter
ρ_i = density of the i-form crystals
ρ_{solv} = density of the solvent
$\sigma_{\mathrm{seed},i}$ = standard deviation for the seed crystal size distribution of i-form crystals

Literature Cited

1. Fujiwara M, Nagy ZK, Chew JW, Braatz RD. First-principles and direct design approaches for the control of pharmaceutical crystallization. *J Process Contr*. 2005;15:493–504.
2. Blagden N, Davey R. Polymorphs take shape. *Chem Brit*. 1999;35:44–47.
3. Brittain HG. The impact of polymorphism on drug development: a regulatory viewpoint. *Am Pharm Rev*. 2000;3:67–70.
4. Hermanto MW, Chiu MS, Woo XY, Braatz RD. Robust optimal control of polymorphic transformation in batch crystallization. *AIChE J*. 2007;53:2643–2650.
5. Roelands CP, Jiang SF, Kitamura M, ter Horst JH, Kramer HJ, Jansens PJ. Antisolvent crystallization of the polymorphs of L-histidine as a function of supersaturation ratio and of solvent composition. *Cryst Growth Des*. 2006;6:955–963.

6. Scholl J, Bonalumi D, Vicum L, Mazzotti M. In situ monitoring and modeling of the solvent-mediated polymorphic transformation of L-Glutamic acid. *Cryst Growth Des*. 2006;6:881–891.
7. Randolph AD, Larson MA. *Theory of Particulate Processes: Analysis and Techniques of Continuous Crystallization*. San Diego: Academic Press, 1988.
8. Sotowa KI, Naito K, Kano M, Hasebe S, Hashimoto I. Application of the method of characteristics to crystallizer simulation and comparison with finite difference for controller performance evaluation. *J Process Contr*. 2000;10:203–208.
9. Hulburt HM, Katz S. Some problems in particle technology: a statistical mechanical formulation. *Chem Eng Sci*. 1964;19:555–574.
10. Singh PN, Ramkrishna D. Solution of population balance equations by MWR. *Comput Chem Eng*. 1977;1:23–31.
11. Briesen H. Hierarchical characterization of aggregates for Monte Carlo simulations. *AIChE J*. 2006;52:2436–2446.
12. Haseltine EL, Patience DB, Rawlings JB. On the stochastic simulation of particulate systems. *Chem Eng Sci*. 2005;60:2627–2641.
13. Ramkrishna D. The status of population balances. *Rev Chem Eng*. 1985;3:49–95.
14. Kumar S, Ramkrishna D. On the solution of population balance equations by discretization. III. Nucleation, growth and aggregation of particles. *Chem Eng Sci*. 1997;52:4659–4679.
15. Qamar S, Warneckea G. Numerical solution of population balance equations for nucleation, growth and aggregation processes. *Comput Chem Eng*. 2007;31:1576–1589.
16. Hounslow MJ, Ryall RL, Marshall VR. A discretized population balance for nucleation, growth, and aggregation. *AIChE J*. 1988; 34:1821–1832.
17. Kumar S, Ramkrishna D. On the solution of population balance equations by discretization. I. A fixed pivot technique. *Chem Eng Sci*. 1996;51:1311–1332.
18. Ma CY, Wang XZ, Roberts KJ. Multi-dimensional population balance modeling of the growth of rod-like L-glutamic acid crystals using growth rates estimated from in-process imaging. *Adv Powder Technol*. 2007;18:707–723.
19. Ma CY, Wang XZ, Roberts KJ. Morphological population balance for modeling crystal growth in face directions. *AIChE J*. 2008;54: 209–222.
20. Puel F, Fevotte G, Klein JP. Simulation and analysis of industrial crystallization processes through multidimensional population balance equations, Part 1: A resolution algorithm based on the method of classes. *Chem Eng Sci*. 2003;58:3715–3727.
21. Harten A. High resolution schemes for hyperbolic conservation laws. *J Comput Phys*. 1983;49:357–393.
22. LeVeque RJ. *Numerical Methods for Conservation Laws*. Basel, Germany: Birkhauser Verlag, 1992.
23. LeVeque RJ. Wave propagation algorithms for multidimensional hyperbolic systems. *J Comput Phys*. 1997;131:327–353.
24. Osher S, Chakravarthy S. High resolution schemes and the entropy condition. *SIAM J Numer Anal*. 1984;21:955–984.
25. Sweby PK. High resolution schemes using flux limiters for hyperbolic conservation laws. *SIAM J Numer Anal*. 1984;21:995–1011.
26. Gunawan R, Fusman I, Braatz RD. High resolution algorithms for multidimensional population balance equations. *AIChE J*. 2004;50: 2738–2748.
27. Ma DL, Tafti DK, Braatz RD. High-resolution simulation of multidimensional crystal growth. *Ind Eng Chem Res*. 2002;41:6217–6223.
28. Qamar S, Elsner MP, Angelov I, Warnecke G, Seidel-Morgenstern A. A comparative study of high resolution schemes for solving population balances in crystallization. *Comput Chem Eng*. 2006; 30:1119–1131.
29. Qamar S, Ashfaqa A, Warneckea G, Angelovc I, Elsnerc M, Seidel-Morgenstern A. Adaptive highresolution schemes for multidimensional population balances in crystallization processes. *Comput Eng*. 2007;31:1296–1311.
30. Woo XY, Tan RBH, Chow PS, Braatz RD. Simulation of mixing effects in antisolvent crystallization using a coupled CFD-PDF-PBE approach. *Cryst Growth Des*. 2006;6:1291–1303.
31. Liu XD, Osher S, Chan T. Weighted essentially non-oscillatory schemes. *J Comput Phys*. 1994;115:200–212.
32. Jiang GS, Shu CW. Efficient implementation of weighted ENO schemes. *J Comput Phys*. 1996;126:202–228.
33. Henrick AK, Aslam TD, Powers JM. Mapped weighted essentially non-oscillatory schemes: achieving optimal order near critical points. *J Comput Phys*. 2005;207:542–567.
34. Serna S, Marquina A. Power ENO methods: a fifth-order accurate weighted power ENO method. *J Comput Phys*. 2004;194:632–658.
35. Hermanto MW, Kee NC, Braatz RD, Chiu MS, Tan RBH. Robust Bayesian estimation of Kinetics for the polymorphic transformation of L-glutamic acid crystals. AIChE J. in press. 2008
36. Mersmann A. *Crystallization Technology Handbook*, 2nd ed. Boca Raton, FL: CRC Press, 2001.
37. Schiesser WE. *The Numerical Method of Lines—Integration of Partial Differential Equations*. New York: Academic Press, 1991.
38. Abdulle A. Fourth order Chebyshev methods with recurrence relation. *SIAM J Sci Comput*. 2002;23:2041–2054.
39. Shu CW. Efficient implementation of essentially non-oscillatory shock-capturing schemes. *J Comput Phys*. 1988;77:439–471.
40. Shu CW. Efficient implementation of essentially non-oscillatory shock-capturing schemes. II. *J Comput Phys*. 1989;83:32–78.
41. Harten A, Engquist B, Osher S, Chakravarthy S. Uniformly high order essentially non-oscillatory schemes. III. *J Comput Phys*. 1987;71:231–303.
42. Fatemi E, Jerome J, Osher S. Solution of the hydrodynamic device model using high order nonoscillatory shock capturing algorithms. *IEEE Trans Comput Aid Des*. 1991;10:232–244.
43. Shu CW. Numerical experiments on the accuracy of ENO and modified ENO schemes. *J Sci Comput*. 1990;5:127–149.
44. Van Leer B. Towards the ultimate conservative difference scheme. II. Monotonicity and conservation combined in a second order scheme. *J Comput Phys*. 1974;14:361–370.
45. Greenough J, Rider W. A quantitative comparision of numerical methods for the compressible Euler equations: fifth-order WENO and piecewise-linear Godunov. *J Comput Phys*. 2004;196:259–281.

Manuscript received Apr. 29, 2008, and revision received July 17, 2008.